ACS APPLIED MATERIALS & INTERFACES

Research Article

Cite This: ACS Appl. Mater. Interfaces 2019, 11, 26127−26133

www.acsami.org

Flexible Self-Powered ZnO Film UV Sensor with a High Response

Qi Xu,[a,‡] Li Cheng,[§] Leixin Meng,[a] Zhe Wang,[∥] Suo Bai,[a] Xiaoqiang Tian,[a] Xiaofeng Jia,[a] and Yong Qin*[,a]

[a]Institute of Nanoscience and Nanotechnology, School of Physical Science and Technology, Lanzhou University, Lanzhou 730000, China

[‡]School of Advanced Materials and Nanotechnology, Xidian University, Xi'an 710071, China

[§]Zhongyuan University of Technology, Zhengzhou, Henan 450007, China

[∥]School of Electrical and Electronic Engineering, Nanyang Technological University, 50 Nanyang Avenue, 639798, Singapore

Supporting Information

ABSTRACT: Response (on/off ratio) is one of the key parameters of ultraviolet (UV) sensors. In this paper, a kind of highly sensitive ZnO UV sensor with highly increased on/off current ratio was designed and developed. Under a weak UV intensity of 0.1 mW/cm^2, this ultrathin ZnO film-based UV sensor has an on/off current ratio of 1.3×10^6 which is 3 times higher than the record value for ZnO-based UV sensors. In addition, it shows good flexibility and stable UV detection property during the bending process. When bending the sensor to a radius of curvature of about 18.5 mm, the sensor also shows high UV detection performance.

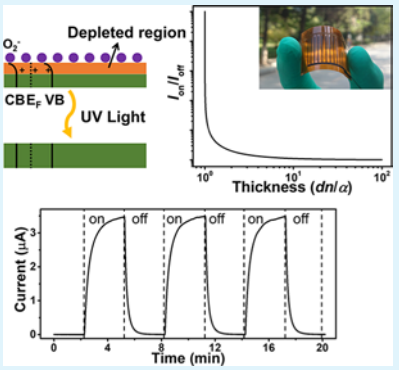

KEYWORDS: *UV sensor, high response, self-powered nanodevice, flexible nanodevice, ZnO film*

INTRODUCTION

Because of the weak and homogeneous background radiation, compared with traditional infrared sensor, ultraviolet (UV) detectors have a higher signal-to-noise ratio and lower working temperature and have been widely applied in many areas, such as flame sensing, UV astronomy, and secure communications.[1−3] In actual application, besides the UV light, the external noise in the environment and internal noise coming from the electrical circuit will also be introduced into the detecting system, which would interfere the signal detection. Sensors with a higher response will contribute to the improvement of the signal-to-noise ratio, sensitivity, etc. which will maintain the sensors in a high quality. Therefore, developing UV sensors with a high response is needed to realize the effective warning of the fire hazard, UV background of the Universe, and establish the low bit error rate communication lines.

ZnO, a biocompatible material[4] with a room temperature band gap of 3.37 eV and exciton binding energy of 60 meV, is a promising candidate for visible-blind UV sensors because of its robust radiation hardness[5,6] and versatile nanostructures such as nanowires, nanobelts, and nanorings.[7−12] ZnO UV sensor's sensing mechanism[13] is based on photogenerated variations in the concentration of surface states. Compared with bulk materials, the micro- and nanostructured ZnO have a much higher surface-to-volume ratio; thus, using them to enhance UV detectors' response has been widely investigated.[14−20] In the study of fabricating micro- and nanostructured ZnO-based UV sensors, the key point is to realize low electron density before UV illumination and high electron mobility. The lower electron density will lead to a lower dark current before UV illumination. The electrons in ZnO can be depleted by surface-adsorbed oxygen[13] or decorated metal nanoparticles with high work function;[21] thus, using nanostructures with a large surface-to-volume ratio is beneficial to obtain a low electron density in ZnO without UV illumination. When illuminated by UV light, the high electron mobility contributes to the increasing photocurrent of sensor. The high electron mobility can be achieved by improving the ZnO's crystallinity, enlarging the grain size and decreasing the cracks, porosity, and so on. With a large surface-to-volume ratio and high electron mobility,[22] ZnO nanowires are commonly used for UV detection.[23−25] Up to now, among ZnO nanowire-based UV sensors, the sensor decorated by Au particles possesses a highest on/off current ratio of 5×10^6 at a UV intensity of 1.3 mW/cm^2.[21] In the past works, the ZnO single-crystal nanomaterials used in UV sensors usually have a size larger than its depletion region's width; thus, the electrons in ZnO are not sufficiently depleted. If the electrons can be fully depleted without UV illumination, the UV sensors' on/off

Received: May 28, 2019
Accepted: June 26, 2019
Published: June 26, 2019

DOI: 10.1021/acsami.9b09264
ACS Appl. Mater. Interfaces 2019, 11, 26127−26133

current ratio may be improved further. Besides the single crystal nanomaterials, the ZnO polycrystal film is another commonly used material to fabricate UV sensors. Compared with the conditions in single-crystal nanomaterials, the oxygen molecules can adsorb on the grain boundary or pores of the film and the electrons can be depleted further. Recently, based on a fully depleted ZnO film, a UV sensor with a high on/off current ratio of 3.4×10^5 at a low UV intensity of 0.1 mW/cm^2 was reported.[26] In that work, the sensor was fabricated by a porous network of nanoparticles with 98% porosity. This porous structure will unavoidably decrease the film's electron mobility, for instance, a typical ZnO nanoparticle-based film shows a low electron mobility of 5×10^{-4} cm^2/V s.[27] Under the dark state, the current is largely determined by the barrier height resulted from the electron depletion between the ZnO grain boundaries; thus, the more the electron is depleted, the lower the dark current is. Under UV illumination, the current is largely determined by the enlarged conducting channel, the higher electron mobility will contribute a higher photocurrent. If a fully depleted film's electron mobility can be improved, a high on/off current ratio can be expected, which will greatly benefit to the development and application of highly sensitive UV sensors.

Here, we developed a kind of flexible UV sensor with a high on/off current ratio based on an ultrathin ZnO film by decreasing the electrons' concentration under dark and increasing the mobility. Under 0.1 mW/cm^2 UV intensity, its on/off current ratio 1.3×10^6 is 3 times higher than the record value 3.4×10^5 of ZnO film-based UV sensors.[26] In addition, under 1 mW/cm^2 UV intensity, its on/off current ratio 3.6×10^7 is 7 times higher than the record value 5×10^6 of ZnO nanowire-based UV sensors[21] under a higher UV intensity of 1.3 mW/cm^2. Furthermore, based on this flexible film, a self-powered UV sensor was developed, which can be used as wearable devices. At the same time, the sensor can work steadily in both flat and curved states with excellent UV detection performance.

RESULTS AND DISCUSSION

Because of the ZnO sensors' surface-related sensing mechanism, the film thickness is very crucial to their performance. In the dark environment, the adsorbed O_2 will consume one electron to form O_2^- adsorbed oxygen ions that will induce a depleted region as shown in the schematic part of Figure 1. Under UV light, the generated holes will migrate to the surface along the potential gradient generated by band-bending to discharge the adsorbed oxygen ions O_2^- and result in the increase of the free carrier concentration and decrease of the depletion width. Suppose, in the dark environment, the surface density of O_2^- is α, the electron density when neglecting the oxygen absorption is n, and the device thickness is d. When UV light is illuminated on the film, the adsorbed O_2 will completely release. Based on above assumptions, without UV illumination, the effective electron density n_1 can be expressed as $n_1 = n - \alpha/d$. Under a constant bias voltage, the current is proportional to the carrier density and mobility; thus the sensor's on/off current ratio can be expressed by $I_{on}/I_{off} = n\mu/(\mu_1 n_1) = (\mu/\mu_1)/(1 - \alpha/(nd))$. μ and μ_1 are the electron mobilities under dark and UV illumination, respectively. The α/n has the dimension of thickness, and it can be considered as the depleted layer of the film caused by the O_2 adsorption. When the film's thickness is close to the depleted layer (α/n), the sensor's on/off current ratio will increase dramatically, which is shown in the simulation curve (Figure 1).

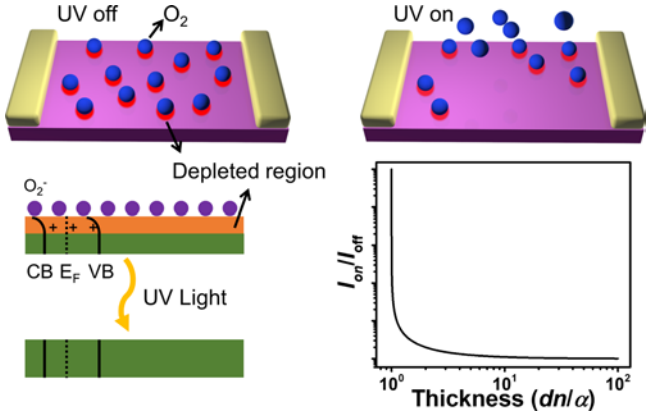

Figure 1. Schematics about the sensing mechanism of ZnO film UV sensor and the on/off current of the film at different thickness supposing that the mobility is invariant under the UV illumination.

After discovering this mechanism, an ultrathin ZnO film was prepared by spin-coating carbon-free aqueous Zn-$(OH)_x(NH_3)_y^{(2-x)+}$ solution on a piranha solution treated glass substrate. First, the glass substrate was treated in the piranha solution (a 3:1 mixture of concentrated H_2SO_4 with 30% H_2O_2), to have the good wettability with the spin-coating solution, which ensures that the solution spreads out evenly on the substrate. Because of ammonia's low viscosity and low volume-loss decomposition process, the synthesized film has a very thin thickness of 19 nm. Almost no cracks, wrinkles, or lumps were found (Figure 2a,b). No contaminants were found in the ZnO ultrathin film (Figure S1). All of the peaks of the grazing incidence XRD pattern can be indexed to the wurtzite crystal structure ZnO (Figure 2c). The interplanar spacing of 0.16, 0.24, and 0.26 nm correspond to the ZnO (110), (101), and (002) facets, respectively (Figure S2a,b). From Figure 2b, it can be seen that there exist small pinholes in the ZnO film,

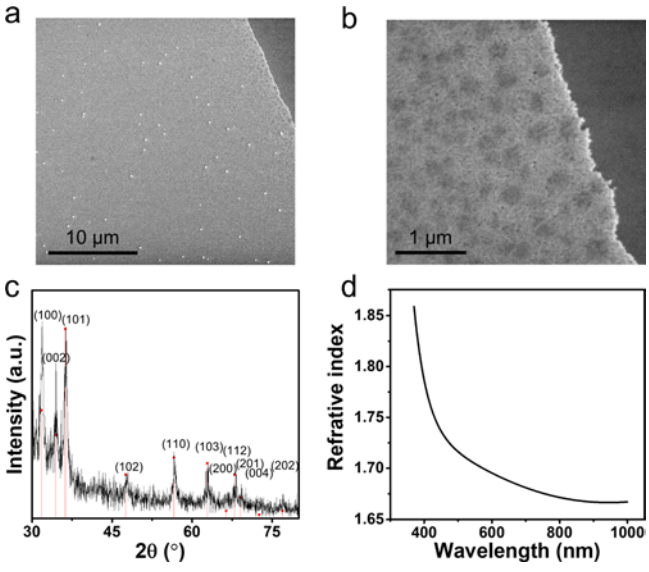

Figure 2. (a,b) SEM images of the ZnO film with different magnifications. (c) X-ray diffraction spectrum of the ZnO film. (d) ZnO film's refractive index at different wavelengths characterized by the spectroscopic ellipsometry.

DOI: 10.1021/acsami.9b09264
ACS Appl. Mater. Interfaces 2019, 11, 26127−26133

which can also be confirmed from the transmission electron microscopy (TEM) image (Figure S2c,d). The void volume fraction was obtained by testing the refractive index by the spectroscopic ellipsometry. The Bruggeman equation (f_v is the relative volume fraction of A; n_A, n_B, and n_h are the refractive index of A, B, and the composite, respectively) $f_v(n_A^2 - n_h^2)/(n_A^2 + 2n_h^2) - (1 - f_v)(n_B^2 - n_h^2)/(n_B^2 + 2n_h^2) = 0$ was used to extract the void volume fraction. After substituting n_A = 1.00 (the air refractive index), n_B = 2.00 at 589 nm,[28] and n_h = 1.70 at 589 nm (Figure 2d), the porosity was determined to be 28.93%. This moderate porosity will contribute to the sensitivity improvement by facilitating the oxygen adsorption/desorption. To characterize the nonuniformity of the film, the film thickness at five different places were tested. Using the measured thickness (Figure S3) and according to the following relation (δ is the nonuniformity; d_{max}, d_{min}, and d_{ave} are the maximum, minimum, and average values of the film thickness, respectively) $\delta = (d_{max} - d_{min})/d_{ave}$; the nonuniformity of the film is calculated to be 10%. As the film is too thin, a small thickness fluctuation will cause a big film nonuniformity.

The transfer characteristics of an ultrathin ZnO film-based field-effect transistor (Figure 3a) fabricated on a silicon substrate was used to obtain the electron mobility. As shown in Figure 3c, exerting positive voltage on the gate electrode can increase the source-to-drain current. This is a typical n-channel field-effect transistor character; thus, the carriers in this device are electrons. The negative shift of the threshold is attributed to the increased electron density under UV, as a more negative voltage should be exerted to the gate electrode to deplete the increased electrons. The relation (I_{ds} is the drain-to-source current, V_{gs} is the gate-to-source voltage, V_{ds} is the drain-to-source voltage, L and W are the length and width of the channel, respectively, and C is the gate insulator capacitance per unit area) $\mu = L(dI_{ds}/dV_{gs})/(V_{ds}WC)$ was used to extract the value of the mobility from the linear part of the $I_{ds}-V_{gs}$ curve (Figure 3c).[29] In dark, the mobility of the ZnO film is 0.19 cm^2/V s which is much higher that of the typical nanoparticle-based film. Combining the calculated electron mobility, $I_{ds}-V_{ds}$ curve (Figure 3b), and channel size, the electron density can also be determined. The electron density in dark is as low as 1.44×10^{12} cm^{-3}. Apart from the electron density, the electron mobility also increases with the UV intensities as shown in Figure 3d. This can be attributed to the decreased grain barriers for the electron to transit between adjacent grains, along with the desorption of adsorbed oxygen molecules in the grain boundaries under UV illumination. According to the former equation, the increased electron mobility under UV illumination will contribute to on/off current ratio improvement, further.

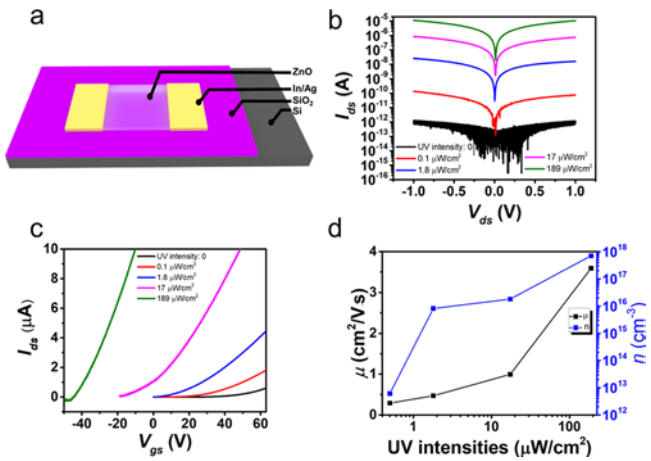

Figure 3. (a) Schematic about the ZnO film-based field-effect transistor. (b) Setting gate voltage to 0 V, the drain-to-source current versus the drain-to-source voltage at different UV intensities. (c) Setting the drain-to-source voltage to 1 V, the drain-to-source current versus the gate-to-source voltage at different UV intensities. (d) Calculated electron mobilities and densities of the ZnO film at different UV intensities.

Based on this film, a UV sensor was fabricated. After ZnO precursor solution was spin-coated on the substrate and annealed, carbon interdigital electrode with an electrode spacing of 500 μm was screen printed on the ZnO film to form a UV sensor. Figure 4a shows the typical $I-V$ curves of the sensor in dark and under UV illumination with an intensity of 1 mW/cm^2. The $I-V$ curves in dark and UV illumination are both linear, which indicates that the carbon electrode forms an Ohmic contact with the ZnO film. At 1 V bias voltage, the dark current is 2.6 pA and the photocurrent is 93.9 μA. This low dark current indicated that most of the electrons in the film are depleted by the surface-adsorbed oxygen molecules. The on/off current ratio is 3.6×10^7, which is 7 times higher than the than the record value 5×10^6 of ZnO nanowire-based UV sensors under an even higher UV intensity of 1.3 mW/cm^2.[21] When the sensor is illuminated with UV intensity of 0.1 mW/cm^2, its photocurrent is 3.49 μA at 1 V bias voltage (Figure 4b). The on/off current ratio is 1.3×10^6, which is 3 times higher than the record value 3.4×10^5 of the ZnO film-based UV sensor.[26] Increasing the length of the electrode spacing will prolong the electrons' carrier transit time. Combing the Ohm's law with the photocurrent expression for the photoconductive UV sensor,[25] it can be found that the photocurrent is inversely proportional to the square of electrode spacing: $I_{on} \propto L^{-2}$. As for the dark current, according to the Ohm's law, the current is inversely proportional to the electrode spacing: $I_{off} \propto L^{-1}$. Therefore, decreasing the electrode spacing will contribute to the increase of the sensor's on/off current ratio. Comparing the electrode spacing of the ultrathin ZnO film-based UV sensors with the sensors possessing record on/off current ratios (2 μm for nanowire-based sensor,[21] 300 μm for thin film-based sensor[26]), the ultrathin film-based sensor will achieve a better on/off current ratio by decreasing the electrode spacing to those values.

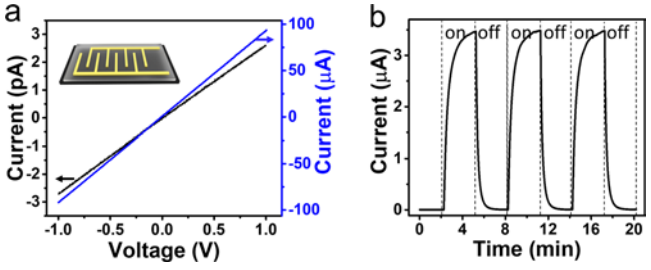

Figure 4. (a) Dark (marked by the left arrow) and photo (marked by the right arrow) $I-V$ characteristics of the device using carbon electrodes. (b) UV response of the sensor illuminated by the 365 nm UV light with an intensity of 0.1 mW/cm^2.

Besides the on/off current ratio, the sensor's rise and decay times, which are used to characterize the time required for the

DOI: 10.1021/acsami.9b09264
ACS Appl. Mater. Interfaces 2019, 11, 26127−26133

current to increase to 90% of the steady-state photocurrent value and to decrease again by 90%, were also characterized. From the time-resolved photocurrent measurements by alternatively exposing the sensor to UV light and dark (Figure 4b), the rise and decay times were computed to be 62.6 and 30.1 s, respectively. These relative long rise and decay times can be ascribed to the slow adsorption/desorption of oxygen molecules from the ZnO film's surface. The sensor's rise time is related to the decreasing rate of the adsorbed oxygen ions O_2^-. When the sensor is illuminated with UV light, because of the surface band-bending, the generated holes will migrate to the surface to neutralize the O_2^- and lead to the desorption of the O_2 molecules. As this process continues, the height of band-bending decreases. The decreased band-bending will slow down the holes' migration speed. Therefore, the rise time is long. The decay time is determined by the velocity of adsorbing O_2 molecules to form O_2^-. After turning off the UV light, the oxygen molecules will gradually adsorb on the ZnO surface; this is a physical process followed by a chemical process. The physical process is driven by the concentration gradient. As the physical process continues, the oxygen density gradient near the ZnO surface decreases. The decreased oxygen density gradient will slow down the oxygen's adsorption, which causes a long decay time.

To expand the sensor's adaptability and sustainability, the self-powered sensor was further designed and developed by constructing Schottky barrier between the ZnO film and electrode. The Schottky barrier between the metal and semiconductor is influenced by work function difference between the metal and semiconductor and the surface state. The surface state varies with the preparation methods of the metal deposition and surface treatment condition; thus, the barrier properties is usually not very reproducible. In contrast to this, the p-type conducting polymer PEDOT:PSS was demonstrated to be a promising Schottky contact candidate, as interfacial trap states may be avoided by the soft fabrication process.[30] Therefore, in this study, the PEDOT:PSS was chosen to form a Schottky barrier with the ZnO film. After ZnO precursor solution was spin-coated on the substrate and annealed, carbon and PEDOT:PSS paste were screen printed, respectively, to form the lower part and upper part of the interdigital electrode. As shown in Figure 5a, when illuminated, the generated electron−hole pairs in the UV sensor space-charge region and nearby will flow in opposite directions in the space-charge region. Holes go to the PEDOT:PSS side and electrons go to the n-type ZnO side. Both contribute to current in the same direction because the electrons are carrying negative charge. This is equivalent to an "extra" reverse current in the Schottky diode; thus, the generated photocurrent will have a negative value. Figure 5b shows typical $I-V$ curves of the sensor in dark and under UV illumination with an intensity of 1 mW/cm^2. The dark current is 0.785 pA at 1 V voltage (Figure 5b). The $I-V$ curve in dark is linear, which is ascribed to the large resistance of depleted ZnO film without UV illumination. Because of the large resistance of the depleted ZnO film, the voltage dropped across the Schottky barrier is relatively low compared with that across the film. Therefore, although at the interface of Schottky contact, the current is exponentially dependent on voltage, because the voltage drop across the Schottky barrier is quite low, the $I-V$ curve is approximately linear. When the film is exposed to UV light, because of the desorption of the oxygen molecules, the conductivity of the ZnO film increases gigantically (about 6

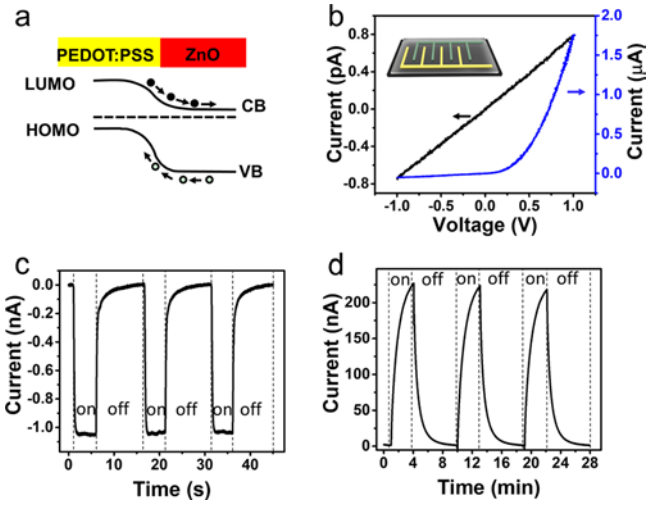

Figure 5. (a) Working mechanism of the self-powered UV sensor. (b) Dark (marked by the left arrow) and photo (marked by the right arrow) $I-V$ characteristics of the devices using a carbon electrode in one end and PEDOT:PSS electrodes in the other end. (c) UV response of the sensor in self-powered mode. (d) UV response of the sensor working at 1 V bias voltage.

orders of magnitude), which greatly decreases the voltage across the ZnO film. Therefore, the voltage dropped across the Schottky barrier becomes quite large, and its rectifying behavior dominates the $I-V$ curve (Figure 5b). When the UV light with an intensity of 0.1 mW/cm^2 was illuminated on the sensor, a 1 nA self-powered current was generated (Figure 5c). Unlike the slow adsorbed oxygen ion-assisted charge separation mechanism, the strong built-in electric field created by the space-charge region will contribute to effective charge separation and result in a faster response time. As for the Schottky contact, the depletion region which mainly resides in the semiconductor side, will form a capacitor as in the case for the electric double-layer capacitor. After the UV light is off, the ZnO film restores to its giant dark resistance, which will lead to a large RC time constant. Therefore, when the UV light is off, the stored charges cannot be released quickly, which lead to a gradually diminished current as shown in Figure 5c. When biased, 204 nA photocurrent was obtained under 1 V voltage (Figure 5d). The on/off current ratio is 2.6×10^5, which is 5 times smaller than that of the sensors with carbon electrodes. This is due to the existence of the Schottky barrier which hinders the electrons' transportation.

Apart from the response, both the on/off current ratio and photocurrent should be linearly dependent on the UV intensities, which is also important to detect and calibrate the intensity of UV light. Therefore, UV photocurrents of the sensor working at 1 V bias voltage and self-powered mode are characterized under a wide range of UV illumination intensities, respectively. At 1 V bias voltage, the lowest tested UV intensity was 100 nW/cm^2. Under that intensity, the photocurrent and on/off current ratio are 430 pA and 548, respectively (Figure 6a). The peak photoresponse current (obtained from the left image of Figure 6a) and the calculated on/off current ratio was plotted as shown in the right part of Figure 6a. The peak photoresponse and on/off current ratio increase monotonously with the UV intensities. A linear regression (red line in the right part of Figure 6a) was applied to the date sets of the on/off current ratio with a coefficient of determination R^2 value of 0.990. This large coefficient indicates

DOI: 10.1021/acsami.9b09264
ACS Appl. Mater. Interfaces 2019, 11, 26127−26133

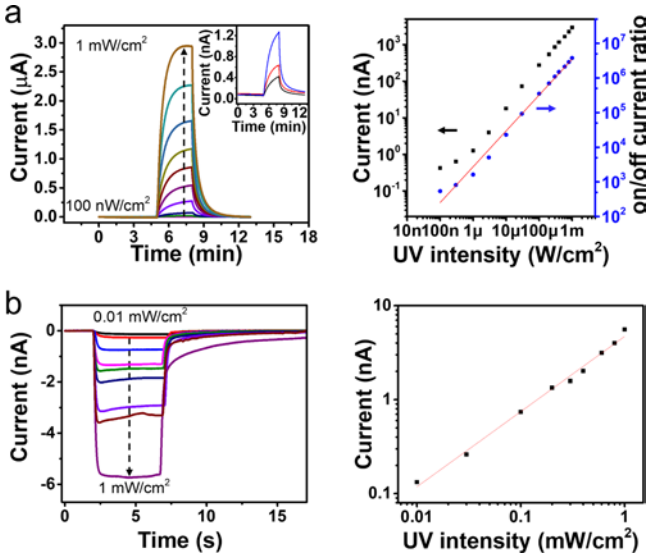

Figure 6. (a) UV response of the sensor working at different UV intensities under 1 V bias voltage; the red line in the right part is a linear fit between the on/off current ratio and UV intensity. (b) UV response of the sensor working at different UV intensities in self-powered mode; the red line in the right part is a linear fit between the photocurrent and the UV intensities.

that there exists a good linearity between the on/off current ratio with the UV intensities. According to this good linearity and the on/off current ratio of 548 at 100 nW/cm^2, the UV sensor could be used to detect even lower UV intensities. At the self-powered mode, the lowest UV intensity tested was 10 μW/cm^2. The peak photoresponse current was obtained from the left image of Figure 6b, and the photocurrent was plotted as shown in the right part of Figure 6b. The peak photocurrent increases monotonously with the UV intensities. A linear regression (red line in the right part of Figure 6b) was applied to the date sets of the photocurrents with a coefficient of determination R^2 value of 0.993. This large coefficient indicates that there also exists a good linearity between the on/off current ratio and UV intensities. The above results show that there exists a good linearity between the photoresponse and UV intensities when the UV sensor works either in a self-powered mode or at 1 V bias voltage. Therefore, the UV intensity can be calibrated conveniently.

Compared with the silicon-based rigid sensors, flexible sensors can be conformally attached on the surface of skins or textile to monitor personal healthcare. The fabricated sensor has a good mechanical flexibility as shown in the inset image of Figure 7a. As for a flexible sensor, apart from its mechanical flexibility, its photoresponse should also be kept when the sensor is bent. To verify whether the sensor's performance can be kept, the sensor's electric properties relating to the UV sensor was tested. First, the sensor's $I-V$ characteristics at the dark environment were characterized at a flat state, bent state with a curvature radius of 18.5 mm, and flat state recovered from the bent state. As shown from Figure 7a, the sensor's $I-V$ curves under three states are nearly identical, which indicates that the sensor's dark current can keep its value when the sensor is in bent state. Next, the sensor's photocurrents at self-powered mode in the above mentioned states were tested as shown in Figure 7b. At the bent state, the sensor's photocurrent is 97.2% of that in the original flat state. After recovering from the bent state to flat state, the sensor's photocurrent is 96.0% of that in the original flat state. Finally, the sensor's photoresponse at 1 V bias voltage was tested at the same procedures as shown in Figure 7c. In the bent state, the sensor's peak current is 99.1% of that in the original flat state. After recovering from the bent state to flat state, the sensor's photocurrent is 97.9% of that in the original flat state. The above results show that the sensor's performance can be kept in the bent state both in self-powered mode and 1 V bias voltage. This can be ascribed to the ultrathin property of the ZnO film, as the thin film has a much less inhomogeneity of stress than that of the thick films.

CONCLUSION

In summary, a flexible UV sensor with the highest reported response was fabricated. Under the UV light of 0.1 mW/cm^2, this sensor possesses an on/off current ratio of 1.3×10^6 which is 3 times higher than the record value for ZnO-based UV sensors. This high on/off ratios is ascribed to the ultralow dark current caused by the film's thickness being close enough to that of the depleted layer and the high photocurrent caused by the high electron mobility. Moreover, a flexible self-powered UV sensor was designed and fabricated. Apart from a good mechanical flexibility, its UV detecting performance can be kept when the sensor was bent to a radius of curvature about 18.5 mm.

EXPERIMENTAL SECTION

Fabrication of ZnO Films and UV Sensors. *ZnO Film Fabrication.* First, the ammine-hydroxo zinc precursor solutions[31] was prepared. In short, NaOH aqueous solution (50 mL 2.5 M) was slowly added dropwise into $Zn(NO_3)_2$ aqueous solution (75 mL 0.5

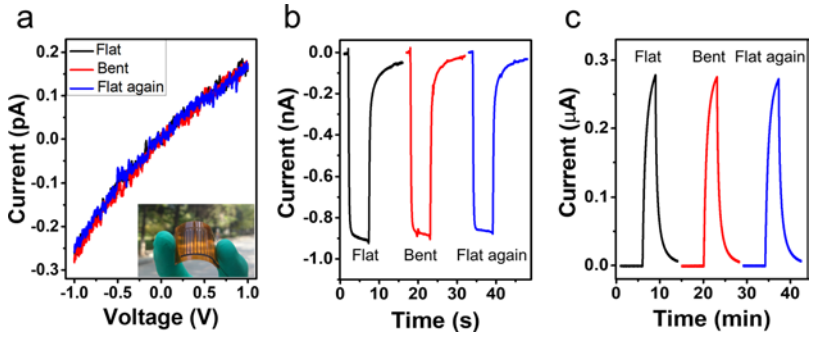

Figure 7. Sensor's performance under flat and curved states. (a) Dark current. (b) Photoresponse at self-powered mode and (c) photoresponse at 1 V bias voltage when the sensor was flat (black), bent (red), and flat again (blue).

DOI: 10.1021/acsami.9b09264
ACS Appl. Mater. Interfaces 2019, 11, 26127−26133

M) under vigorously stirring. After being centrifuged and removing the supernatant of the resulting hydroxide slurry five times, the hydrated precipitate was dissolved in ammonia (250 mL 6.6 M) to form the precursor solution. Second, the substrate (glass and Kapton film) was cleaned with acetone, alcohol, and deionized water in sequence to remove all contaminants on its surface. Then, the substrate was treated in piranha solution (a 3:1 mixture of concentrated H_2SO_4 with 30% H_2O_2) for 3 h to make them possess a good hydrophilic property, and then the precursor solutions were spin-coated on the substrate at a rate of 1000 rpm for 30 s. It was cured on a 100 °C hot plate for 20 min, followed by thermal annealing at 150 °C for 2 h in air.

Sensors Fabricated on Glass Substrates. First, a screen-printing stencil with an interdigital electrode pattern was made to order. The interdigital electrode pattern consists of two interlocking comb-shaped arrays. For each comb-shaped array, the fingers have a width of 500 μm and adjacent spacing of 1500 μm. Second, the screen-printing stencil was placed atop a glass substrate covered with the ZnO film and the carbon ink was put on top of the stencil, using a squeegee to push the ink through the pattern on the stencil to form a carbon interdigital electrode on the ZnO film. Finally, it was baked on an 80 °C hot plate for 60 min to solidify the electrode. The schematic fabrication process can be seen in Figure S4a. The sensor has a size of 22 mm × 17 mm.

Sensors Fabricated on the Kapton Substrate. First, two screen-printing stencils were made to order. Each screen has comb-shaped arrays with a finger width of 500 μm and n adjacent spacing of 1500 μm. The comb-shaped patterns on the two stencils have a mirror symmetry to each other. Second, a screen-printing stencil was placed atop a Kapton substrate covered with the ZnO film and the carbon ink was put on top of the stencil, using a squeegee to push the ink through the pattern on the stencil to form a carbon comb-shaped array electrode on the ZnO film, followed by thermal baking at 80 °C for 60 min. After that, the other screen-printing stencil was placed atop the Kapton substrate covered with the ZnO film during which the pattern of 50 μm shifted downward to that of the early printed carbon electrode and the PEDOT:PSS ink was put on top of the stencil, using a squeegee to push the ink through the pattern on the stencil to form a PEDOT:PSS comb-shaped array electrode on the ZnO film, followed by thermal baking at 80 °C for 60 min. The schematic fabrication process can be seen in Figure S4b. The two kinds of comb-shaped array electrodes are interlocked to form an interdigital electrode on the ZnO film. The sensor has a size of 22 mm × 17 mm.

ZnO Film's Field-Effect Transistor Fabrication. The ZnO film was fabricated on a heavily doped n-type silicon substrate with a silicon oxide layer using the technique described in the ZnO film fabrication part. Then, the In/Ag electrode was deposited on the ZnO film through a standard shadow mask process. The SiO_2 layer thickness on the silicon substrate is 285 nm, and the width and length of the channel are 0.3 and 4 mm, respectively.

UV Sensor Characterization. All of the electrical measurements including $I-V$ curve, dark current, and photoresponse were performed using DS345 30 MHz synthesized function generator and SR 570 low-noise current preamplifier. The UV light intensity was quantified by a UV detector (Photoelectric Instrument Factory of Beijing Normal University, UV-A).

ZnO Film's Thickness and Nonuniformity Test. First, the ZnO film was fabricated on a 2 cm × 2 cm glass substrate. Second, a layer of SU-8 photoresist was spin-coated on it. A strip array shadow mask was placed with both width and spacing equal to 1 mm, and it was exposed to the UV light. Then, the photoresist was washed in acetone, alcohol, and water, subsequently. An array of photoresist stripes with a width of 1 mm was fabricated on the film. Finally, it was dipped into dilute HCl solution, acetone, alcohol, and water, in sequence to obtain an array of ZnO stripes. Finally, the film thickness at five different places with a dice 5 pattern was tested using a atomic force microscope (AFM). The four corner points of the dice 5 pattern span an area of 2 mm × 2 mm. Using the above measured thickness (Figure S3) and according to the following relation (δ is the nonuniformity; d_{max}, d_{min}, and d_{ave} are the maximum, minimum, and average values of the tested thickness, respectively) $\delta = (d_{max} - d_{min})/d_{ave}$, the nonuniformity of the film is calculated. The average value is considered as the film thickness.

■ ASSOCIATED CONTENT

Supporting Information

The Supporting Information is available free of charge on the ACS Publications website at DOI: 10.1021/acsami.9b09264.

EDX spectrum; TEM, high resolution TEM, element mapping; AFM topography images; and schematics about the sensors made on the glass substrate and Kapton substrate (PDF)

■ AUTHOR INFORMATION

Corresponding Author

*E-mail: qinyong@lzu.edu.cn.

ORCID

Yong Qin: 0000-0002-6713-480X

Author Contributions

Qi Xu and Li Cheng contributed equally. The manuscript was written through contributions of all authors. All authors have given approval to the final version of the manuscript.

Notes

The authors declare no competing financial interest.

■ ACKNOWLEDGMENTS

We sincerely appreciate the support from NSFC (no. 51472111), the National Program for Support of Top-notch Young Professionals, the Fundamental Research Funds for the Central Universities (no. JB181402, no. lzujbky-2018-ot04).

■ REFERENCES

(1) Monroy, E.; Calle, F.; Pau, J. L.; Muñoz, E.; Omnès, F.; Beaumont, B.; Gibart, P. AlGaN-Based UV Photodetectors. *J. Cryst. Growth* **2001**, *230*, 537−543.

(2) Goldberg, Y. A. Semiconductor Near-Ultraviolet Photoelectronics. *Sci. Technol.* **1999**, *14*, R41−R60.

(3) Razeghi, M.; Rogalski, A. Semiconductor Ultraviolet Detectors. *J. Appl. Phys.* **1996**, *79*, 7433−7473.

(4) Li, Z.; Yang, R.; Yu, M.; Bai, F.; Li, C.; Wang, Z. L. Cellular Level Biocompatibility and Biosafety of ZnO Nanowires. *J. Phys. Chem. C* **2008**, *112*, 20114−20117.

(5) Burlacu, A.; Ursaki, V. V.; Lincot, D.; Skuratov, V. A.; Pauporte, T.; Rusu, E.; Tiginyanu, I. M. Enhanced Radiation Hardness of ZnO Nanorods versus Bulk Layers. *Phys. Status Solidi Rapid Res. Lett.* **2008**, *2*, 68−70.

(6) Auret, F. D.; Goodman, S. A.; Hayes, M.; Legodi, M. J.; van Laarhoven, H. A.; Look, D. C. Electrical Characterization of 1.8 MeV Proton-Bombarded ZnO. *Appl. Phys. Lett.* **2001**, *79*, 3074−3076.

(7) Wang, Z. L. Nanostructures of Zinc Oxide. *Mater. Today* **2004**, *7*, 26−33.

(8) Qiu, Z.; Wong, K. S.; Wu, M.; Lin, W.; Xu, H. Microcavity Lasing Behavior of Oriented Hexagonal ZnO Nanowhiskers Grown by Hydrothermal Oxidation. *Appl. Phys. Lett.* **2004**, *84*, 2739−2741.

(9) Wang, Z. L.; Kong, X. Y.; Zuo, J. M. Induced Growth of Asymmetric Nanocantilever Arrays on Polar Surfaces. *Phys. Rev. Lett.* **2003**, *91*, 185502.

(10) Vayssieres, L. Growth of Arrayed Nanorods and Nanowires of ZnO from Aqueous Solutions. *Adv. Mater.* **2003**, *15*, 464−466.

(11) Yatsui, T.; Kawazoe, T.; Ueda, M.; Yamamoto, Y.; Kourogi, M.; Ohtsu, M. Fabrication of Nanometric Single Zinc and Zinc Oxide Dots by the Selective Photodissociation of Adsorption-Phase

DOI: 10.1021/acsami.9b09264
ACS Appl. Mater. Interfaces 2019, 11, 26127−26133

Diethylzinc Using a Nonresonant Optical Near Field. *Appl. Phys. Lett.* **2002**, *81*, 3651−3653.
(12) Huang, M. H.; Mao, S.; Feick, H.; Yan, H. Q.; Wu, Y. Y.; Kind, H.; Weber, E.; Russo, R.; Yang, P. D. Room-Temperature Ultraviolet Nanowire Nanolasers. *Science* **2001**, *292*, 1897.
(13) Jin, Y.; Wang, J.; Sun, B.; Blakesley, J. C.; Greenham, N. C. Solution-Processed Ultraviolet Photodetedtors Based on Colloidal ZnO Nanoparticles. *Nano Lett.* **2008**, *8*, 1649−1653.
(14) Kind, H.; Yan, H.; Messer, B.; Law, M.; Yang, P. Nanowire Ultraviolet Photodetectors and Optical Switches. *Adv. Mater.* **2002**, *14*, 158−160.
(15) Zhou, J.; Gu, Y.; Hu, Y.; Mai, W.; Yeh, P.-H.; Bao, G.; Sood, A. K.; Polla, D. L.; Wang, Z. L. Gigantic Enhancement in Response and Reset Time of ZnO UV Nanosensor by Utilizing Schottky Contact and Surface Functionalization. *Appl. Phys. Lett.* **2009**, *94*, 191103.
(16) Sharma, P.; Sreenivas, K.; Rao, K. V. Analysis of Ultraviolet Photoconductivity in ZnO Films Prepared by Unbalanced Magnetron Sputtering. *J. Appl. Phys.* **2003**, *93*, 3963−3970.
(17) Lao, C. S.; Park, M.-C.; Kuang, Q.; Deng, Y.; Sood, A. K.; Polla, D. L.; Wang, Z. L. Giant Enhancement in UV Response of ZnO Nanobelts by Polymer Surface-Functionalization. *J. Am. Chem. Soc.* **2007**, *129*, 12096.
(18) Liu, X.; Gu, L.; Zhang, Q.; Wu, J.; Long, Y.; Fan, Z. All-Printable Band-Edge Modulated ZnO Nanowire Photodetectors with Ultra-High Detectivity. *Nat. Commun.* **2014**, *5*, 4007.
(19) Jin, Z.; Gao, L.; Zhou, Q.; Wang, J. High-Performance Flexible Ultraviolet Photoconductors Based on Solution-processed Ultrathin ZnO/Au Nanoparticle Composite films. *Sci. Rep.* **2014**, *4*, 4268.
(20) Chen, M.; Hu, L.; Xu, J.; Liao, M.; Wu, L.; Fang, X. ZnO Hollow-Sphere Nanofilm-Based High-Performance and Low-Cost Photodetector. *Small* **2011**, *7*, 2449−2453.
(21) Liu, K.; Sakurai, M.; Liao, M.; Aono, M. Giant Improvement of the Performance of ZnO Nanowire Photodetectors by Au Nanoparticles. *J. Phys. Chem. C* **2010**, *114*, 19835−19839.
(22) Goldberger, J.; Sirbuly, D. J.; Law, M.; Yang, P. ZnO Nanowire Transistors. *J. Phys. Chem. B* **2005**, *109*, 9−14.
(23) Liu, J.; Wu, W.; Bai, S.; Qin, Y. Synthesis of High Crystallinity ZnO Nanowire Array on Polymer Substrate and Flexible Fiber-Based Sensor. *ACS Appl. Mater. Interfaces* **2011**, *3*, 4197−4200.
(24) Das, S. N.; Moon, K.-J.; Kar, J. P.; Choi, J.-H.; Xiong, J.; Lee, T. I.; Myoung, J.-M. ZnO Single Nanowire-Based UV Detectors. *Appl. Phys. Lett.* **2010**, *97*, 022103.
(25) Soci, C.; Zhang, A.; Xiang, B.; Dayeh, S. A.; Aplin, D. P. R.; Park, J.; Bao, X. Y.; Lo, Y. H.; Wang, D. ZnO Nanowire UV Photodetectors with High Internal Gain. *Nano Lett.* **2007**, *7*, 1003−1009.
(26) Nasiri, N.; Bo, R.; Wang, F.; Fu, L.; Tricoli, A. Ultraporous Electron-Depleted ZnO Nanoparticle Networks for Highly Sensitive Portable Visible-Blind UV Photodetectors. *Adv. Mater.* **2015**, *27*, 4336−4343.
(27) Sun, B.; Sirringhaus, H. Solution-Processed Zinc Oxide Field-Effect Transistors Based on Self-Assembly of Colloidal Nanorods. *Nano Lett.* **2005**, *5*, 2408−2413.
(28) Haynes, W. *CRC Handbook of Chemistry and Physics*, 97th ed.; CRC Press: Boca Raton, Florida, 2016; pp 10−251.
(29) Zhou, X.; Zhang, Q.; Gan, L.; Li, H.; Zhai, T. Large-Size Growth of Ultrathin SnS_2 Nanosheets and High Performance for Phototransistors. *Adv. Funct. Mater.* **2016**, *26*, 4405−4413.
(30) Nakano, M.; Tsukazaki, A.; Gunji, R. Y.; Ueno, K.; Ohtomo, A.; Fukumura, T.; Kawasaki, M. Schottky Contact on a ZnO (0001) Single Crystal with Conducting Polymer. *Appl. Phys. Lett.* **2007**, *91*, 142113.
(31) Meyers, S. T.; Anderson, J. T.; Hung, C. M.; Thompson, J.; Wager, J. F.; Keszler, D. A. Aqueous Inorganic Inks for Low-Temperature Fabrication of ZnO TFTs. *J. Am. Chem. Soc.* **2008**, *130*, 17603−17609.

DOI: 10.1021/acsami.9b09264
ACS Appl. Mater. Interfaces 2019, 11, 26127−26133